Iranian Journal of Astronomy and Astrophysics
Vol. 10, No. 1, Winter 2023, 123–138
©Available online at http://ijaa.du.ac.ir
DOI: 10.22128/ijaa.2023.714.1158
Online ISSN: 2383–403X

Iranian Journal of Astronomy and Astrophysics

Research Paper

A Comparison Between Cool Chromospheric and Hot Coronal Jets

Ehsan Tavabi[1] · Azam Molla Tayefeh*[2]

[1] Physics Department, Payame Noor University (PNU), Tehran, P.O.Box 19395-3697, Iran;
email: e_tavabi@pnu.ac.ir

[2] PhD Student, Payame Noor University (PNU), Tehran, Iran;
*email: azam.mollatayefeh@gmail.com

Received: 22 August 2023; **Accepted:** 27 September 2023; **Published:** 2 October 2023

Abstract. Spicules and jets occur in a typical emerging magnetical collimated flux tube, and we examine polar surges through limb observations in two wavelengths, revealing a more distinct view of the dynamic events high above the polar cap's chromosphere. Magnetic flux tube plays a key role and a wide range of jet-like activities in the solar atmosphere. The observational characteristics of these mass ejections are reviewed, and unified model based on magnetic reconnection or other alternative is presented to account for these different plasma ejections. Several excellent time sequences of images were taken with the Hinode Solar Optical Telescope (SOT) through the HCaII K and Hα line broadband filter and also X-Ray Telescope (XRT) with high spatial and temporal resolution was used. Image processing include the use of a mad-max operator is used to reveal and improve the visibility of hair-like futures (especially for chromospheric small-scale anemone jets) and to a specific plasma motion in the vicinity of the X-null point. The intensive and rapid temporal observations imply a tight connection between Surges and similar jet-like phenomena, corroborating the theory that the acceleration and upward movement of these events are propelled by magnetic reconnection triggered by the emergence of flux.

Keywords: Sun, Chromosphere, Jets, Transition Region

1 Introduction

The dynamics of the magnetical emerging flux are dominated by jets. The jets are essential and they may have a clue to solve chromospheric and coronal heating and accelerated high-speed solar wind some the small scale structures observed in the solar wind may be related to these jets [1]. They can be classified in two distinguishable groups, (i) cool plasma jets which include chromospheric structures such as spicule, spike, macro-spicule, and surges ([2–4]), (ii) and also hot plasma ejection, such as EUV coronal, X-ray jets, and x-ray plasmoid ([5–8]).

X-ray jets have been discovered on the Sun by the soft X-ray telescope aboard the Japanese Yohkoh satellite as transitory x-ray enhancement in the solar corona with collimated motion ([5]). An abundance of evidence exists for magnetic reconnection in x-ray jets and also the SXT observations that confirm about 10 of them exhibit helical structure

* *Corresponding author*

([9]). Furthermore, magnetic twist is a visible candidate for the initiation of the jet ([10,11]). Hinode SOT shows the ubiquitous presence of chromospheric anemone jets in the HCaII line in active regions ([12]). The general shape of these small-scale jets is similar to the Eiffel tower (or Lambda shape), same as x-ray coronal hole jets.

Spicules are hair-like structures seen above the solar limb in many optically thick chromospheric lines. The dynamics and evolution of spicules are most exciting and remain unresolved yet. In their initial appearance, they appear geyser-like in the sense that there is an upward motion of collimated material, after reaching a typical maximum height (10,000 km), the ejection stops, and is followed by a fading of the spicule brightness or return of the emitting material to the photosphere. At least, two different types of spicule have been introduced by De Pontieu et al. (2007) [13]. The type-II spicules are extremely fluid, develop apparent faster and disappear over their whole length within a few seconds. $H\alpha$ surges have been studied over 60 years (see Roy 1973, [14]), they are straight ejections that reach peak velocity 50-200 kms^{-1}. They reach heights of 200 Mm, and the typical lifetime about of 10-20 min.

Several researchers have established a connection between surges and large spicules (macrospicules) through magnetic reconnection. Kurokawa & Kawai (1993) [15] studied the morphology and evolutionary traits of surges occurring near emerging flux tubes, deducing that these events arise from magnetic field reconnection between the emerging flux tube and the preexisting surrounding area. Gaizauskas (1996) [16] provided an instance of a surge observed in Hα, reinforcing the concept that magnetic reconnection serves as the driving force behind the acceleration mechanism of this phenomenon.

Some other authors suggest that the phenomena we call Hα surges (cool) and X-ray jets (hot) are closely related in certain events. Models of surges can be classified according to the magnetic tension force, this force results from magnetic reconnection and gives rise to the slingshot motion. Other models, such as twisted magnetic field lines have been advanced by Shibata and Uchida (1986) [17] to explain surges, and Hollweg et al. (1982) [18] to explain spicule.

Georgakilas et al. (2001) [19] examined the dynamics of the surge, and their findings align with the models proposed by the reconnection theory. Their analysis provides robust backing for the notion that magnetic reconnection, induced by emerging flux, serves as the driving force behind the acceleration of such jets. Another potential explanation involves the shearing effect, resulting from the intermediate-scale photospheric motion of the footpoints of the underlying intricate magnetic field structure, as a trigger for the eruption ([20]).

Observations in HCaII and $H\alpha$ filtergrams of SOT onboard on the Hinode telescope show cold and dense plasma ejections. This structure has almost reported using the ground-base observation in $H\alpha$ line and historically call surges. Apart from the differences in scale and some other physical parameters, there is a strong similarity between a spicule and a surge ([21]) and seem that spicules and surges are due to the same formation mechanism.

Surge typically has the form of a straight or slightly curved spike (or macrospicule) which grows upward from the chromosphere (presumably near 1 to 2 Mm above the photosphere). They ascend with a wide range of velocity, with an average apparent velocity of about 50-500 kms^{-1} and almost reaches a typical height of 20,000-200,000 km and then falls back to the chromosphere, the lifetime is in the ranges from 10 minutes to 2 hours ([22]). Some observation reports suggest that cool chromospheric surges and coronal jets are closely related to each other ([22–24]).

A diverse array of dynamic occurrences within the solar atmosphere, such as soft X-ray jets and distinct flares, have been linked to magnetic reconnection taking place within a three-dimensional magnetic null point configuration, featuring a fan plane beneath the null point and an overlying spine field line (e.g. Priest & Forbes 2000 [25]).

In cases of potential or nearly potential magnetic fields, the introduction of a magnetic bipole into one polarity region of a larger bipolar ambient field leads to the spontaneous emergence of a three-dimensional null point arrangement, complete with a fan and a spine ([20]). It is generally accepted that reconnections are appropriate for explaining features such as particle acceleration and plasma heating. The unique characteristics of X-type neutral points have been pivotal in shaping the progression of X-ray evolution.

Magnetic energy accrues within current sheets at null points within the plasma, serving as loci for potent magnetic energy release ([25]). Craig & Fabling (1996) [26] suggested that current sheets are associated mainly with three-dimensional fan-current reconnection, other reconnection model requires quasi-cylindrical spine currents that develop along the exhaust axis of the fluid ([27]).

Furthermore, there exists observational support for magnetic reconnection in surges, exemplified by phenomena like the lambda-shaped, whip-like motion, which is construed as a slingshot-like effect stemming from reconnection. Even rotational motion can be attributed to reconnection between a twisted flux tube and an untwisted flux tube ([28]).

Coronal X-ray jets are believed to occur when reconnection between emerging ropes (the 2D simulations Yokoyama & Shibata 1996 [29]), the recent 3D reconnection simulation had been performed by Moreno-Insetis et al. (2008) [30] and fan-spine topology formation through two-step reconnection is driven twisted flux emergence is investigated in detail using 3D simulation by Torok et al. 2010 [31], was successful in reproducing several key observation aspects of coronal jets. However, these simulations could not explain the most important feature of jets which exhibit helical structure and untwisting ([11]), and more recently, the clear demonstration of twisted structure from stereoscopic observations of polar jets compares favorably with synthetic images from a recent MHD simulation invoking magnetic untwisting as their driven mechanism reported by Patsourakos et al. (2008) [10]. On the other hand, chromospheric explosive events seen in cool emission lines may represent small scale reconnection is the same as flare-like (or plasmoid ejections) reconnection in the corona and due to the expansion of the single helical flux rope into the solar upper atmosphere. However, of course, the principal effect of the current in a face-free field (fff) is to introduce a twist, or helicity, into the field structure. The curl of a helical field has a component in the direction of the field itself. The helical structure of fff approximation is investigated by Sakurai (1979) [32].

The origin of the helical structure must be sought in a rotation of the field-line footpoints. An exciting aspect of the fff is that its energy exceeds the energy of the potential field belonging to the same chromospheric boundary conditions. Increasing twist therefore means increasing the storage of field becomes unstable. The stored excess energy could be released in a explosive event.

Magnetic reconnection due to collisions of two parts of twisted flux rope can produce helical motion such as surge-like ejection and this helix jets are strongly showing re-ordering of field lines behavior after emerging from the null point site is a natural consequence of magnetic helicity conservation ([33]). Van Ballegooijen (1999) [34] attributed the origin of magnetic twist to the effects of random flows (granulation and supergranulation) after they emerge through the launched site.

2 Observations and Image Processing

2.1 Data Reduction

Hinode XRT and SOT data acquired from different solar limb locations have been employed to investigate the dynamic characteristics of solar jets. The XRT serves as a high-resolution grazing-incidence telescope, and comprehensive information regarding its instrumentation and capabilities can be found in Golub's work (2007) [35].

The XRT imagery showcased in this research (Figure 2) was captured using the Ti-poly filter, boasting a field of view (FOV) of $512'' \times 512''$ and an approximate spatial resolution is around $2''$ ($1''.032\ pixel^{-1}$). The HCaII Utilized data in this work from the Broadband Filter Imager (BFI) of SOT and $H\alpha$ data from the Narrowband Filter Imager (NFI) was used [36].

The observations were conducted continuously for several minutes, varying in cadence from 3 to 10 seconds, utilizing a diffraction limit of λ/D at $0''.16$ (equivalent to 120 km) for the Ca line. The pixel size was $0''.054$. In comparison, the spatial resolution and diffraction limit for $H\alpha$ were approximately twice as fine, at $0''.33$ (equivalent to 250 km), with a pixel size of $0''.08$.

The utilized images all possess dimensions of 1024×512 pixels squared, with Hinode selectively reading only the central pixels of the detector to maintain a high cadence, aligning with telemetry constraints. As a result, the covered field of view (FOV) spans $111'' \times 56''$. Calibration of the Hinode SOT and XRT data was executed using standard "fg_prep" and "xrt_prep" software, as outlined in Shimizu ([37]).

Enhanced spatial processing of linear features is achieved by implementing the mad-max algorithm [38]. The mad-max operator significantly enhances the finest scale structure, operating as a weakly nonlinear modification of a spatial filter based on the second derivative. Specifically, it amplifies the maximal variation in the second derivative across various directions, substantially emphasizing linear structures. This technique mitigates the merging of intersecting threads that are aligned along the line of sight, similar to the effect of a second derivative, but with a more pronounced focus on the direction of maximum variation. The original algorithm sampled the second derivative in eight directions, but in this study, the directional variability of the second derivative was extended to a smooth function with an adjustable spatial scale passband (For further details, refer to November & Koutchmy (1996) [39]). The application of the "mad-max" algorithm in spatial filtering reveals distinctively bright radial threads within the chromosphere, approaching the resolution limit of approximately 120 km.

A superior spatial image processing for line-like features is obtained using the mad-max algorithm [38]. The mad-max operator acts to improve the finest scale structure substantially. The mad-max filter is a weakly nonlinear modification of a second derivative spatial filter. Mainly, it is where the second derivative has a maximum when looking along different directions. The behavior of the mad-max qualitatively resembles the second derivative, but the strong selection for the direction of the maximum variation substantially enhances line-like structure. It reduces blending between crossing threads superposed along the line of sight. The algorithm, as initially proposed, samples the second derivative in eight directions, but the directional variation of the second derivative was generalized to a smooth function with a selectable passband spatial scale for this work (for more details, see the November & Koutchmy 1996 [39]).

The Hinode SOT data at various positions on a solar limb have been used to study dynamical nature of the jets. The HCaII data used in this study from the Broadband Filter Imager (BFI) of SOT and H data from the Narrowband Filter Imager (NFI) was used ([36]).

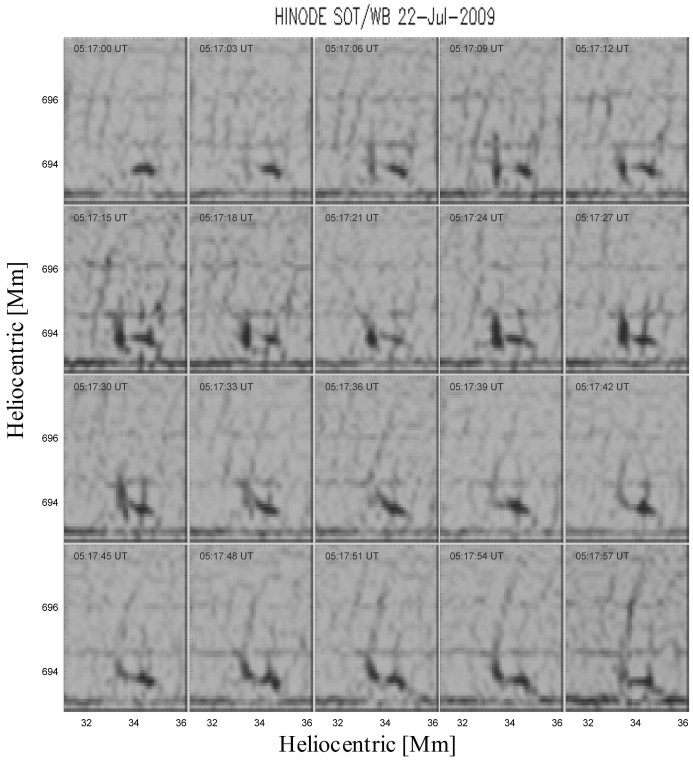

Figure 1: Negative and mad-maxed Ca images showing the time evolution of a typical Ca jet, times are shown in UT.

2.2 Event Description

The brightening of several loop systems at the edge of the Sun was observed by SOT for about 10 min on 2007 Nov. 07, between about $17:46$ and $17:57 UT$. Figure 2&3 shows snapshots outlining the main feature of the jet in two HCaII and Hα lines simultaneously, about of 17 : 50 UT, the multicomponent jet part become visible (the red braid-like fine threads) the green line denoted the average axis of the surge (including the interchange space) and double thin green lines show the boundary of the surge with the distance of 3 Mm. The arcades rose up slowly, and then the threads were rapidly emerging, and the redial expansion of the jet is occurring, after reaching the maximum height, the threads started to fall back to the left as whip-like behavior (for more details, see the snapshots poster in Figure 1).

At the beginning of the ejection phase, several expanding arcades are seen at the surge footpoint and after ejecting, the whip-like motion is also obviously seen during surge evolution (Figure 1, 17 : 51). Despite the ambiguity of the sense of direction, it is very appealing that the appearance of the observed surge should be explained by the introduction of a magnetic right-handed twist of 3π to 4π angle, this helix angle amount is most apparent in $H\alpha$ line images (Figure 2).

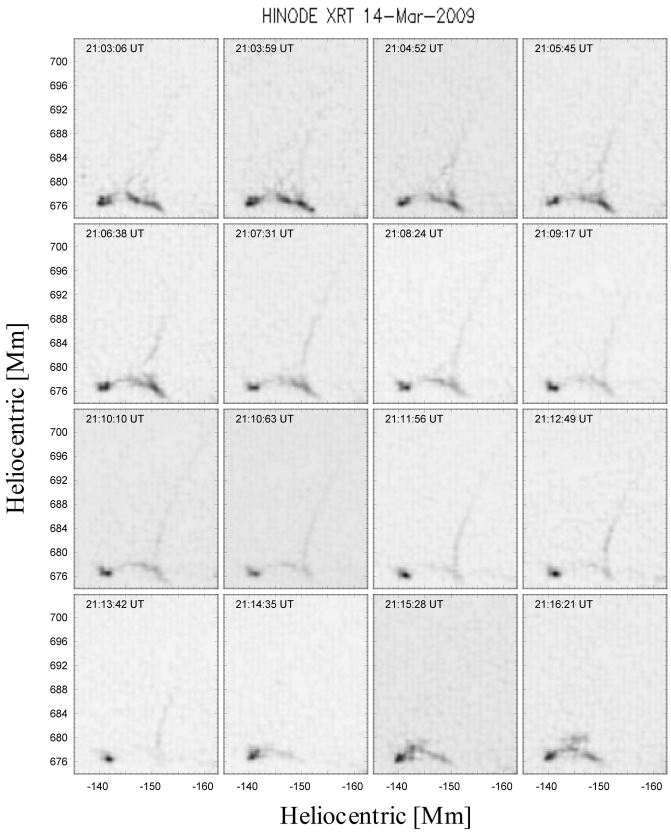

Figure 2: Negative and mad-maxed X-ray images showing the jet evolution on 14 March 2009.

3 Discussion and Results

We have developed an algorithm to identify solar spicules in the first-ever systematic survey of off-disk spicules using exclusively Mg II spectral observations. Here, primarily based on the Interface Region Imaging Spectrograph (IRIS) data from the poles and equator. These are raster and image slit jaw data. The IRIS exhibits a spatial precision ranging from 0.3 to 0.4 arcseconds, and each pixel measures 0.166 arcseconds. The data encompasses a spectral span stretching from the near ultraviolet (NUV) to the far ultraviolet (FUV), encompassing the range of 1389 to 2834 A [40]. Doppler map computations and spicule separation are performed using raster images related to the Mg II k broadband and Si iv 1400 A spectra, respectively. In order to compare chromospheric anemone Ca jet and other jet-like structures the Hinode high cadence image is available now.

Figure 1 shows the time evolution of a typical Ca small-scale jet, which was obtained using high cadence ($3 \sim 4sec$), the observed morphology of small-scale chromospheric jet, such as the lambda-shape, suggesting that they are related to magnetic reconnection. This

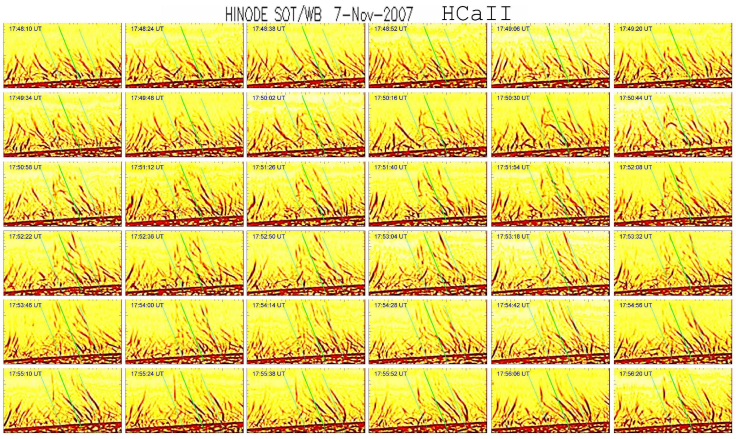

Figure 3: A Ca surge in the polar region, all Images intensity inverted and processing using mad-max

configuration (X-type null point reconnection) was extended to consider X-ray jet in the corona by Shibata (1994) [41] and Filippov (1999) [42].

Magnetic reconnection is an all-encompassing physical phenomenon, capable of unfolding across various spatial and temporal dimensions ([25]); its manifestations span from the chromosphere and photosphere to the corona [43]. The lifetime of the Ca jet is very short, less than $45sec$, and its size is smaller than X-ray jets. Their maximum height of them is about $6Mm$, and the length of their footpoint is no longer than $1.5Mm$.

The apparent (projected) velocity of them is about $200kms^{-1}$, which is comparable with the velocity of a coronal hole X-ray jet ([11]). A faintly visible part of a jet is shown in the frames of Figure 2, all these similarities between Ca and x-ray jets suggest that their formation mechanism should be the same. Jets may be related to other dynamic phenomena such as surges. Surges are almost cool plasma jets and are usually observed in $H\alpha$ at ground-based observation, space observations (such as with EUV telescope) also detect Surges. Surges are ejected at peak velocities of $50 - 200kms^{-1}$, and magnetic field of surges are continuously accelerated during the ascent phase and show a spinning motion. It is difficult to discriminate large surges from sprays, which are non-collimated cool plasma ([44]).

Also, there is some observation evidence for magnetic reconnection in surges, such as the lambda-shape, whip-like motion which is interpreted as a slingshot-like motion as a result of reconnection, even spinning motion can be interpreted as a result of reconnection between a twisted flux tube and an untwisted flux tube ([28]), we report on the first HcaII line observation of a typical polar surge simultaneously to the $H\alpha$ taken by Hinode SOT in Figures 3 and 4. The position of this phenomenon has been shown in Figure 5 (big arrow). Blake & Sturrock (1985)[45] proposed the concept that spicules, macrospicules, and surges represent manifestations of a unified phenomenon unfolding across distinct scales. In their investigation, they endeavored to identify a mechanism capable of elucidating these events across various scales. Their proposition entailed the necessity of two distinct magnetic field configurations: one susceptible to reconnection, serving as the propulsive force, and the other responsible for guiding and accounting for the focused mass ejection.

The structure and movement of the observed surges and jets necessitate a reconnection framework in which magnetic tension and the release of twisted energy contribute significantly. Convincing indications of reconnection are offered by whip-like movements, and the

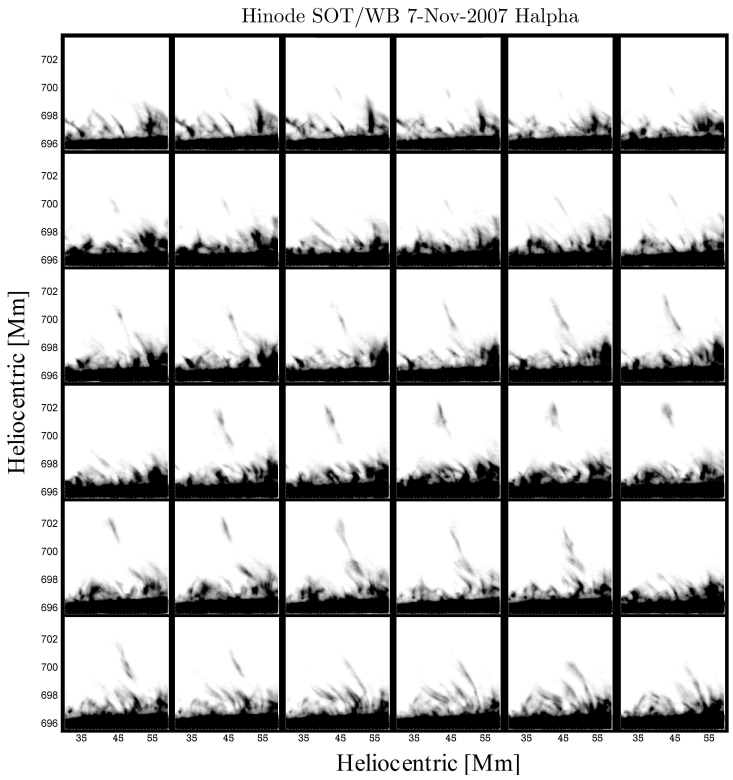

Figure 4: A *Ca* surge in the polar region, all Images intensity inverted and processing using mad-max

rotational behavior of the surges (refer to detailed spinning motion in Figure 3 at higher resolution and also Figure 4 for lower spatial resolution) arises as an outcome of the relaxation of reestablished magnetic twist.

Prior to Yokoyama & Shibata's (1993, 1995) [46,47] two-dimensional numerical simulation of solar X-ray jets grounded in a reconnection framework connecting emerging flux and preexisting coronal magnetic fields, it was conventionally believed that the ejection of cool $H\alpha$ plasma could not be attributed to reconnection due to the anticipated heating of such plasma to high X-ray temperatures. In their proposed model, four distinct types of jet flows are associated with the process of reconnection: a hot jet following magnetic field lines, a slingshot jet, a simple island ejection, and a surge cool jet. In Figure 5 we could also see many double jet-like features or double threads. Tanaka (1974) found that about 30% of all dark disc mottles are double, and Suematsu et al. (2008) reported that most spicules (more than 50%) show up double threads structure during their evolution (see small arrows in Figure 5) [48,49].

The IRIS spectra spicules to determine one of the factors affecting the production and feeding of solar winds [50]. Jets and spicules have been considered by examining several raster frames from the regions of the Sun. The shifted positions from the original spectrum were previously discovered independently in the Mg II k 2796 A. The characteristics of spicules, such as the rotational velocity of each spicule concerning the central axis of the spectrum (Figures 6 and 7) , were computed using the output of the Doppler map. Then, using the Mg II spectrum simultaneously, Doppler maps for specific index samples were

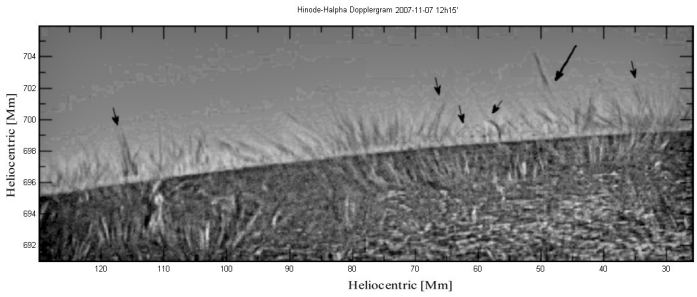

Figure 5: Spicules at the limb taken with the H narrowband Dopplergram of SOT. The image was processed to enhance visibility by the mad-max operator, and is negative. Big arrow showing the surge, which was shown in Figures 3 and 4, this image with high resolution shows a lot of double threads (indicated by small arrows).

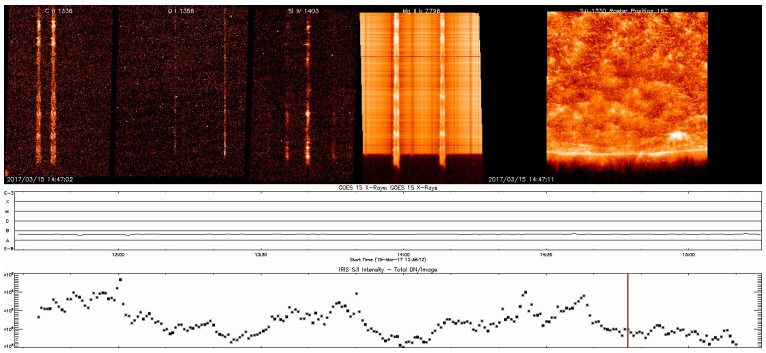

Figure 6: IRIS NUV spectrum off-limb taken on 15 March 2017 at 14:47 UT. The two strong emission lines are Mg ii k 2796°A and Mg ii h 2803°A (middle part), both formed over a range of heights from the upper photosphere to the upper chromosphere. This wavelength range also contains a multitude of photospheric lines, and 1400 SJI images (Si IV band, right panel) at the limb, the goes X-ray detector is also seen.

created at various speeds. Based on the results, a speed of 30 km/s was demonstrated in Figure 8. Note that the impact of various projection angles on the edges and sky has been disregarded (Figure 8-b).

The technique was applied to identify spicules with a heightened likelihood of being twisted, as indicated by closely juxtaposed red and blue shifts oriented in opposite directions within the twisted spicules. The process involved employing an algorithm to identify regions in a matrix with identical values. The velocities mapped onto the Doppler map were categorized into three values: red, white, and blue, which corresponded to -30, 0, and +30 km/s, respectively. This entailed the utilization of a Doppler map matrix. This matrix could be employed to locate specific values and regions with a strong potential for twisted spicules (areas, where consecutive blue and red shifts were observed were selected as instances of twisted spicules). These rotating spicules were selected from the Doppler maps, and their spatial, temporal, and spectral attributes were subsequently compared with the resulting

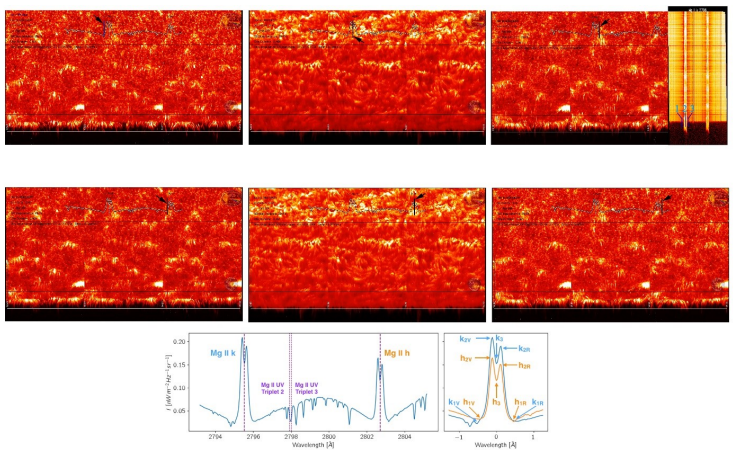

Figure 7: IRIS reconstructed 2796°A images above the limb taken on 15 March 2017 at 14:47 UT. These images are sensitive to plasma of the upper chromosphere (2796°A) and upper photosphere (2830°A). The upper chromospheric image also contains contributions from the upper photosphere to the middle chromosphere, which are dominant in more quiet regions. The dark vertical line in the Mg II h and k spectral is shown on the images (top part) and shows the spectrum wavelength to extract these images. The top right panel shows the center and wings of the Mg II h resonance line. Bottom left panel display that the Mg k line has an oscillator strength twice as large as that the Mg h line, and at $= 1$ the peaks of the Mg k line are located at more considerable heights than the Mg h line, where the source function is larger. For a given line, e.g., either Mg II h or k, the profile can have its left peak higher than the right one owing to a downflow. Inversely, if the right peak is higher, then this is due to an upflow. The bottom right panel display the intensity of these profile features used to diagnose temperatures; the wavelength of these profile features (or separation between them) used to diagnose velocities or velocity gradients and the ratio between the difference of peak intensities and the sum of peak intensities to determine downflows or upflows

properties. The Mg II k spectrum is used to create Doppler maps. The Mg II k spectrum (see Figure 8) is employed for this, and at a specific velocity, a Doppler map is created. The Doppler map is then modified with the features of the regions where the possibility of twisted spicules are the greatest.

In these designated regions, the data's spatial resolution measures 0.3193 arcseconds and 0.1589 arcseconds, respectively. During Doppler map computations, the Doppler velocity is computed with a precision of 1 km/s. These resolutions are deemed sufficient for conducting accurate spatial and wavelength analyses. The spiral motion along these jets, delineated by spectral tilting angles and intricately structured magnetically confined plasma, could effectively capture and extend the background material, propelling plasma upward into the higher solar atmosphere. The magnetic field entrapped within the spiral imparts an initial disturbance, propelling the plasma along the helical medium to generate a seemingly spontaneous ejection within the solar atmosphere. Numerous observations and investigations underscore that tornado-like outbursts, including surges, consist of elongated, fine threads [52,53]. Ultimately, the nuanced structure we report, exemplified by helical chromospheric jets, complicates our comprehension of the transition from the corona to the substantial contribution of fast solar wind. The pivotal Alfvén surface likely possesses a rather intricate and essentially helical configuration. Given the anticipated interplay between wavelength

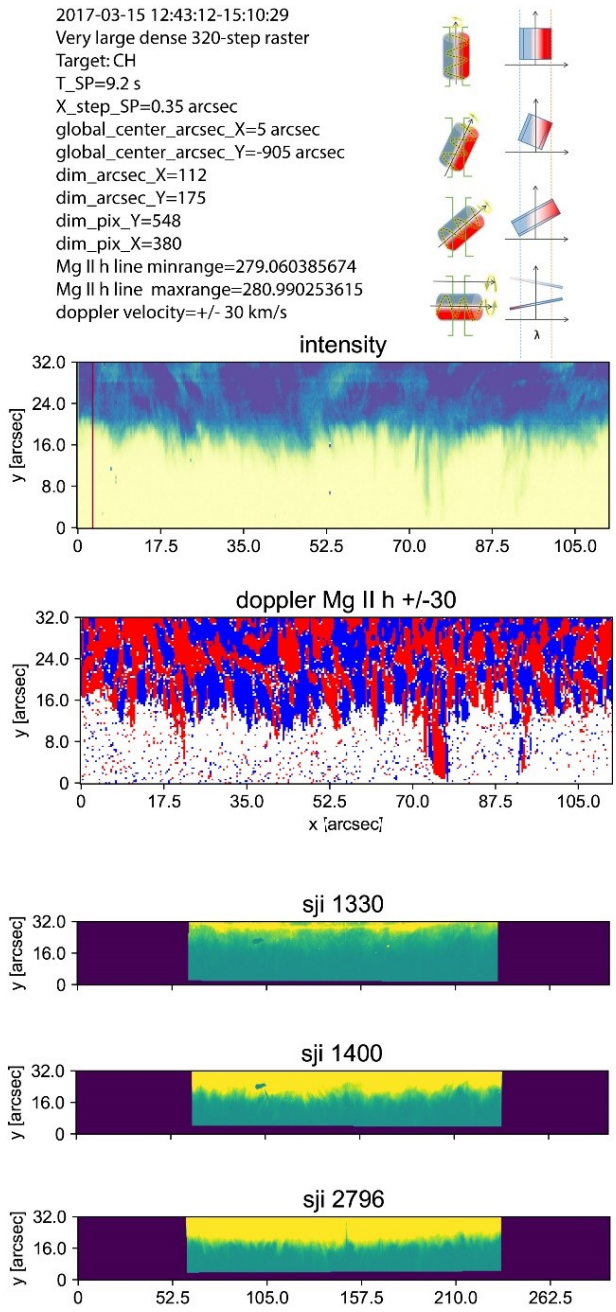

Figure 8: These graphs are produced with a resolution of 0.35 arcsec south pole region and the simultaneous intensity map. The Doppler velocity slices taken from the Mg II k spectra at +/-30 km/s velocities for the Pole are shown, and the velocities range are +/-30 km/s decorated from the blue for -30km/s, white for 0km/s, and red for +30km/s. The moving slit jaw images in three channels are illustrated as bottom panels.

and the effective Alfvén speed, it is more appropriate to envision this rotational behavior as an Alfvén wave in which information flows inward. At least, a subset of these mechanisms accelerates plasma to fuel the fast solar wind within polar regions. Although significant efforts have gone into investigating the origins and sources of solar winds, but the underlying mechanics remain unresolved. Over the years, researchers have identified several mechanisms responsible for generating solar wind [54–59]. Most of them thought the occurrence at the poles was particularly effective in generating solar wind [60].

The solar wind is a steady stream of electrons and charged particles. Solar winds are divided into two types: fast solar wind and slow solar wind. These two groups differ in terms of particle origin, speed, temperature, and density. So, they are distinguishable not just by their associated speeds but also significantly by their thermodynamic and compositional properties; their related sources at the Sun must have different sources. The slow solar wind has less Alfvénicity than the fast solar wind, and the Alfvénicity is more evident in the fast wind. The degree of Alfvénicity of these winds is mainly dependent on their source, which is why winds with coronal hole origins correlate more to Alfvén [53,61,62].

The fast solar winds materialize within the coronal holes positioned at the solar poles, where magnetic field lines are exposed [64]. In order for plasma to escape the Sun's gravitational pull, it must be tethered to magnetic field lines are extending into interplanetary space. The pivotal mechanism driving the acceleration and discharge along these 'open' field lines holds the key to identifying the coronal origins of the fast solar wind. Spicules, characterized by their pointed structures, are frequently observed in the chromosphere and the transition region (TR) of the Sun. These features were initially identified by Father Secchi [51] and are clearly evident in the spectra of Mg II k& h, C II, Ca II H, and Si IV [13,65–70]. The first instance of macrospicules was recorded in $HeII\lambda304$ and $H\alpha$ images by [71]. Approximately, 23 years later, Pike & Mason (1998) revealed that macrospicules displaying blue and red shifts in opposing directions exhibit a spiral motion [72]. Our investigation into spicules unveiled a distinctive type that deviates from prior observations regarding speed, angle, and direction of movement. These spicules appear to result from vortical movements, which could also contribute to the propagation of Alfvén rotational waves and the transfer of energy to the Sun's upper atmosphere. It is essential to acknowledge the varying observational resolutions in this study and to recognize that rotating spicules represent minute structures observable in exceedingly high-resolution imaging.

Acknowledgments

The authors express their appreciation to NASA for providing access to IRIS solar data accessible to the general public. Our gratitude extends to the Hinode team for the accessibility of their data. Additionally, we are thankful for the valuable insights provided by the late Prof. Serge Koutchmy, which significantly influenced the direction of our research. The image processing software known as OMCsoftware (commonly referred to as Mad-max) was developed for IDL and is readily downloadable from the late O. Koutchmy's UPMC website at http://www.ann.jussieu.fr/ koutchmy/debruitage/madmax.pro.

Authors' Contributions

All authors have the same contribution.

Data Availability

No data available.

Conflicts of Interest

The authors declare that there is no conflict of interest.

Ethical Considerations

The authors have diligently addressed ethical concerns, such as informed consent, plagiarism, data fabrication, misconduct, falsification, double publication, redundancy, submission, and other related matters.

Funding

This research did not receive any grant from funding agencies in the public, commercial, or nonprofit sectors.

References

[1] Feldman, W. C., Gosling, J. T., McComas, D. J., & Phillips, J. L. 1993, JGR, 98, 5593.

[2] Sterling, H. C. 2000, Sol. Phys., 196, 79.

[3] Koutchmy, S., & Stellmacher, G. 1976, Sol. phys., 49, 253.

[4] Shibata, K. 1998, Ap&SS, 264, 129.

[5] Shibata, K., Ishido, Y., Acton, L., Strong, K., Hirayama, T., Uchida, Y., & et al. 1992, PASJ, 44, L173.

[6] Tsuneta, S. 1997, ApJ, 483, 507.

[7] Koutchmy, S., Hara, H., Suematsu, Y., & Reardon, K. 1997, A&A, 320, L33.

[8] Koutchmy, S., Hara, H., Shibata, K., Suematsu, Y., & Reardon, K. 1998, A&A, 320, L33.

[9] Shimojo, M. 1996, ApJ, 464, 1016.

[10] Patsourakos, S., Pariat, E., Vourlidas, A., Antiochos, S. K., & Wuelser, J. P. 2008, ApJ, 680, L73.

[11] Filippov, B., Golub, L., & Koutchmy, S. 2009, Sol. Phys., 254, 259.

[12] Shibata, K., Nakamura, T., Matsumoto, T., Otsuji, K., Okamoto, T., Nishizuka, N., & et al. 2007, Science, 318, 1591.

[13] De Pontieu, B., McIntosh, S., Hansteen, V., Carlsson, M., Schrijver, C., Tarbell, T., & et al. 2007, PASJ, 59, S655.

[14] Roy, J. R. 1973, Sol. phys., 28, 95.

[15] Kurokawa, H., & Kawai, G. 1993, ASP Conf. Ser., 46, 507.

[16] Gaizauskas, V. 1996, Sol. Phys., 169, 357.

[17] Shibata, K., & Uchida, Y. 1986, Sol. Phys., 103, 299.

[18] Hollweg, J. V., Jackson, S., & Galloway, D. 1982, Sol. Phys., 75, 35.

[19] Georgakilas, A. A., Koutchmy, S., & Christopoulou, E. B. 2001, A&A, 370, 273.

[20] Antiochos, S. K., DeVore, C. R., & Klimchuk, J. A. 1999, ApJ, 510, 485.

[21] Tandberg-Hanssen, E., 1974, Solar Prominences, GAAM, 12.

[22] Liu, Z., Pagani, M., Zinniker, D., DeConto, R., Huber, M., Brinkhuis, H., Shah Walter, S., Leckie, M. & Pearson, Ann. 2009, Science EOT dataset.

[23] Schmider, F., Fossat, E., Grec, G., & Gelly, B. 1988, Advances in Helio and Asteroseismology, 1988, 123.

[24] Jiang, C., Honma, I., Kudo, T., & Zhou, H. 2007, Electrochem. Solid State Lett., 10, 5.

[25] Priest, E. R., & Forbes, T. G. 2000, Magnetic Reconnection, Cambridge Univ. Press, Cambridge.

[26] Craig, I. J. D., & Fabling, R. B. 1996, ApJ, 462, 969.

[27] Galsgaard, K., & Nordlund, Å. 1997, J. Geophys. Res., 102, 231.

[28] Canfield, R. C., Reardon, K. P., Leka, K. D., Shibata, K., Yokoyama, T., & Shimojo, M. 1996, ApJ, 464, 1016.

[29] Yokoyama, T., & Shibata, K. 1996, PASJ, 48, 353.

[30] Moreno Insertis, F., Galsgaard, K., & Uggarte-Urra, I. 2008, ApJ, 673, 211.

[31] Toeroek, T., Aulanier, G., Schmieder, B., Reeves, K. K., & Golub, L. 2009, ApJ, 704, 485.

[32] Sakurai, T. 1979, PASJ, 31, 209.

[33] Berger, M. A. 1999, Magnetic Helicity in Space and Laboratory Plasmas, Geophys. Monograph 111, A.G.U., 1.

[34] Van Ballegooijen, A. A. 1999, Magnetic Helicity in Space and Laboratory Plasmas, Geophys. Monograph, 111, 213.

[35] Golub, L., DeLuca, E., Austin, G., Bookbinder, J., Caldwell, D., Cheimets, P., Cirtain, J., & et al. 2007, Sol. Phys., 243, 63.

[36] Tsuneta, S., Ichimoto, K., Katsukawa, Y., Nagata, S., Otsubo, M., Shimizu, T., Suematsu, Y., & et al. 2008, Sol. Phys., 249, 167.

[37] Shimizu, T., Nagata, S., Tsuneta, S., Tarbell, T., Edwards, C., Shine, R., & et al. 2008, Sol. Phys., in press.

[38] Koutchmy, O., & Koutchmy, S. 1989, in Proc. 10th Sacramento Peak Summer Workshop, High Spatial Resolution Solar Observations, ed. O. von der Luhe (Sunspot: NSO), 217.

[39] November, L. J., & Koutchmy, S. 1996, ApJ, 466, 512.

[40] De Pontieu, B., Title, A. M., Lemen, J. R., Kushner, G. D., Akin, D. J., Allard, B., & et al. 2014, Sol. Phys., 289, 2733.

[41] Shibata, K., Nitta, N., Strong, K. T., Matsumoto, R., Yokoyama, T., Hirayama, T., Hudson, H., & Ogawara, Y. 1994, ApJ, 431, 51.

[42] Filippov, B. 1999, Sol. Phys., 185, 297.

[43] Litvinenko, Y. E. 1999, ApJ, 515, 245.

[44] Shibata, K., Copyright © Nature Publishing Group 2001 Brunel Road, Houndmills, Basingstoke, Hampshire, RG21 6XS, UK Registered No. 785998 and Institute of Physics Publishing.

[45] Blake, M. L., & Sturrock, P. A. 1985, ApJ, 290, 359.

[46] Yokoyama, T., & Shibata, K. 1993, in ESA, Fourth International Tokio Conference on Plasma Physics and Controlled Nuclear Fusion, 203.

[47] Yokoyama, T., & Shibata, K. 1996, PASJ, 48, 353.

[48] Tanaka, K. 1974, IAUS, 56, 239.

[49] Suematsu, Y., Ichimoto, K., Katsukawa, Y., Shimizu, T., & Okamoto, T. 2008, ASPC, 397, 27.

[50] Tavabi, E., Koutchmy, S., & Ajabshirizadeh, A. 2012, EAS Publications Series, 55, 71.

[51] Secchi, P. A. 1877, Le Soleil, 2, Chap. II. Paris: Gauthier-Villars.

[52] Chen, H. D., Zhang, J., & Ma S. L. 2012, RAA, 12, 573.

[53] Tavabi, E., Koutchmy, S., & Golub, L., 2015, SoPh., 290, 2871.

[54] Parker, E. N. 1958, ApJ, 128, 664.

[55] McComas, D. J., Barraclough, B. L., Funsten, H. O., Gosling, J. T., Santiago-Muñoz, E., Skoug, R. M., & et al. 2000, JGR Space Physics, 105, 10419.

[56] Stakhiv, M., Landi, E., Lepri, S. T., Oran, R., & Zurbuchen, T. H. 2015, ApJ, 801, 100.

[57] Kepko, L., Viall, N. M., Antiochos, S. K., Lepri, S. T.,Kasper, J. C., & Weberg, M. 2016, Geophysical Research Letters, 43, 4089.

[58] Abbott, B. P., Abbott, R., Abbott, T. D., Abernathy, M. R., Acernese, F., Ackley, K., & et al. 2016, Phsical Review Letters, 116, 061102.

[59] DeForest, C. E., Howard, R. A., Velli, M., Viall, N., & Vourlidas, A. 2018, ApJ, 862, 18.

[60] Krieger, A. S., Timothy, A. F., & Roelof, E. C. 1973, Sol. Phys., 29, 505.

[61] Geiss, J., Gloeckler, G., & Von Steiger, R. 1995, Space Science Reviews, 72, 49.

[62] Von Steiger, R., Schwadron, N. A., Fisk, L. A., Geiss, J., Gloeckler, G., Hefti, S., & et al. 2000, JGR Space Physics, 105, 27217.

[63] Schwenn, R. 2006, Space Science Reviews, 124, 51.

[64] Hassler, D. M., Dammasch, I. E., Lemaire, P., Brekke, P., Curdt, W., Mason, H. E., & et al. 1999, Science, 283, 810.

[65] Sterling, A. C., Moore, R. L., & DeForest, C. E. 2010, ApJ, 714, L1.

[66] Madjarska, M. S., Vanninathan, K., & Doyle, J. G. 2011, A&A, 532, L1.

[67] Pereira, T. M. D., De Pontieu, B., Carlsson, M., Hansteen, V., Tarbell, T. D., Lemen, J., & et al. 2014, ApJ, 792, L15.

[68] Pereira, T. M. D., De Pontieu, B., & Carlsson, M. 2012, ApJ, 759, 18.

[69] Pereira, T. M. D., Rouppe van der Voort, L., & Carlsson, M. 2016, ApJ, 824, 65.

[70] Beck, T., Tao, Ch., Chen, L., & Frank, S. 2016, Journal of Banking & Finance, 72, 28.

[71] Moore R. L., Tang F., Bohlin J. D. & Golub L. 1977, ApJ, 218, 286.

[72] Pike, C. D., & Mason, H. E. 1998, Sol. Phys., 182, 333.